

FeF_2 cathode.⁵ This was attributed to the formation of $\text{Fe}_x\text{Li}_{2-2x}\text{F}_2$.

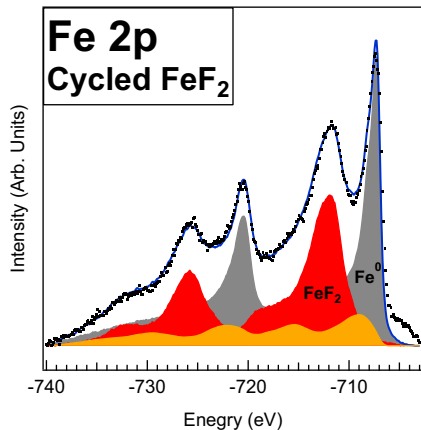


FIG. S3: Fe 2p XPS spectrum from a cycled FeF_2 cathode showing the same spectral components as the thin film sample.⁶

The formation of $\text{Fe}_x\text{Li}_{2-2x}\text{F}_2$ was also observed in recent *ex situ* XPS measurements of electrochemically cycled FeF_2 electrodes.⁶ Figure S3 shows the peak fitting scheme used for a delithiated electrode in this previous work. These measurements showed that the $\text{Fe}_x\text{Li}_{2-2x}\text{F}_2$ did not fully dissociate upon the delithiation of the electrode, and hence this ternary compound might be partially responsible for the capacity losses observed in FeF_2 cells.

III. EVOLUTION OF IRON PEAKS

The reduction of the FeF_2 film upon exposure to lithium was quantified by fitting the Fe 2p peak with a sum of Fe^0 , FeF_2 , and $\text{Fe}_x\text{Li}_{2-2x}\text{F}_2$ components. Figure S4 shows the evolution of the normal emission Fe 2p spectra for several different lithium exposures. The spectra have been normalized by their maximum intensities in order to highlight their visual differences. From these spectra, it can be seen that the relative intensities of the Fe^0 and $\text{Fe}_x\text{Li}_{2-2x}\text{F}_2$ components increase monotonically as a function of lithium exposure, while the FeF_2 intensity simultaneously decreases. The $\text{Fe}:\text{Fe}_x\text{Li}_{2-2x}\text{F}_2$ ratio increases slightly as a function of exposure, from 0.85 after 5 minutes of exposure to 1.10 after 160 minutes.

IV. ARXPS DETAILS

The model used to fit the $R(\theta, d)$ curves consisted of an infinitely thick film of FeF_2 with an inhomogeneously thick overlayer of $\text{Fe}_x\text{Li}_{2-2x}\text{F}_2$ and Fe metal, as shown in Figure S5. In order to model the attenuation of the FeF_2 photoelectrons, the overlayer was divided vertically into four different types of regions: (1) thick Fe^0 , (2) thick

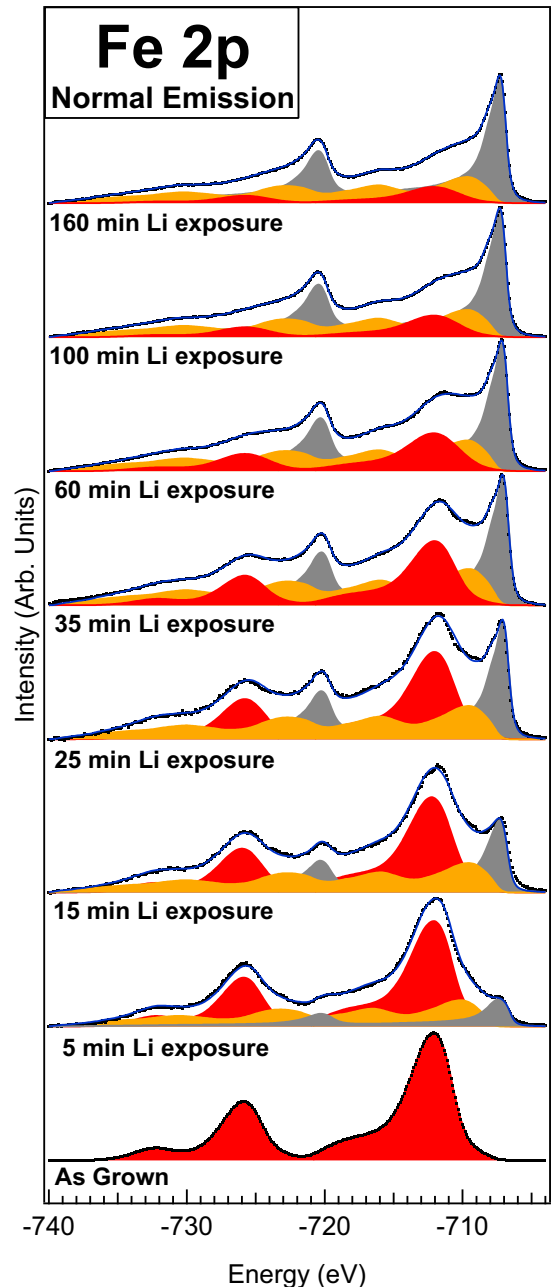


FIG. S4: Fe 2p spectra of the FeF_2 film taken at normal emission after each lithium exposure.

$\text{Fe}_x\text{Li}_{2-2x}\text{F}_2$, (3) thin Fe^0 , and (4) thin $\text{Fe}_x\text{Li}_{2-2x}\text{F}_2$. The relative coverages of Fe^0 and $\text{Fe}_x\text{Li}_{2-2x}\text{F}_2$ were determined by the ratio of the specific volume of each species, such that 85% of the surface was covered by $\text{Fe}_x\text{Li}_{2-2x}\text{F}_2$ and 15% by Fe^0 . This columnar geometry of overlayer compounds is consistent with the Fe^0 and $\text{Fe}_x\text{Li}_{2-2x}\text{F}_2$ spectral intensities being equal for all angles and overlayer thicknesses.

The FeF_2 signal was then calculated from the following

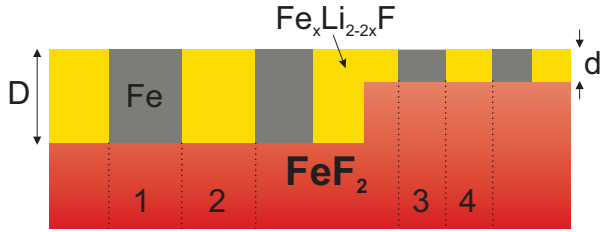


FIG. S5: Model of the Li-FeF₂ conversion reaction used to generate $R(\theta, d)$ curves. The FeF₂ substrate is divided into four distinct regions of overlayer thicknesses and compositions.

equation:⁷

$$I_{\text{FeF}_2}(d, \theta) = I_{\text{FeF}_2}^{\infty} \sum_{i=1}^4 \Theta_i \left[\exp \left(-\frac{d_i}{\lambda_i(d, \theta) \cos \theta} \right) \right] \quad (\text{S1})$$

where Θ_i is the fractional coverage of each region and $\lambda_i(d, \theta)$ was calculated for each species, thickness, and emission angle using a procedure described below. Similarly, the Fe⁰ and Fe_xLi_{2-2x}F₂ signals were then calculated by:

$$I_{\text{Fe}}(d, \theta) = I_{\text{Fe}}^{\infty} \sum_{i=1}^4 \Theta_i \left[1 - \exp \left(-\frac{d_i}{\lambda_i(d, \theta) \cos \theta} \right) \right]. \quad (\text{S2})$$

The ratio R was then calculated as

$$R(\theta, d) = \frac{I_{\text{Fe}}(d, \theta)}{I_{\text{FeF}_2}(d, \theta)}. \quad (\text{S3})$$

The effective attenuation lengths were calculated using the NIST EAL Calculator.⁸⁻¹¹ Table SI shows the EALS calculated at normal emission for each species. Similar tables were calculated at each 5° increment from 0 – 50°.

SV. STRUCTURAL PARAMETERS

FeF₂ has a P4₂/mmn rutile (tetragonal) structure with lattice constants $a = b = 4.697 \text{ \AA}$ and $c = 3.309 \text{ \AA}$ at

d (nm)	λ_{FeF_2} (nm)	λ_{Fe} (nm)	$\lambda_{\text{Fe}_x\text{Li}_{2-2x}\text{F}_2}$ (nm)
0.2	1.44	1.04	2.35
0.4	1.42	1.03	2.33
0.6	1.41	1.01	2.32
0.8	1.40	1.01	2.30
1.0	1.40	1.00	2.29
2.0	1.38	0.98	2.26
3.0	1.36	0.96	2.24
4.0	1.35	0.95	2.23
5.0	1.35	0.96	2.22

TABLE SI: Effective attenuation lengths of each iron compound calculated at normal emission using the NIST EAL Database.

room temperature. Each Fe²⁺ ion in the bulk is bound to six F⁻ ions in a distorted octahedral configuration with metal-ion distances of 2.03 Å and 2.10 Å.¹² The FeF₂ [110] channels have nearly square cross sections and are located between the octahedra in the lattice. This square cross section measures 2.10×2.10 Å, from the centers of the fluorine ions at the boundaries. Including the radii of the F⁻ ions, the cross section of the [110] channel is approximately 0.6 Å, which is smaller than the diameter of either Li⁰ or Li⁺. This geometrical argument supports the assertion that lithium cannot diffuse into the FeF₂(110) surface. In comparison, the FeF₂ [001] channels are 3.43×3.43 Å from the centers of the bounding ions and 2.18×2.18 Å including the ionic radii, which is large enough to accommodate either Li⁰ or Li⁺ diffusion.

Element	Charge	Radius (pm)
Li	0	145
Li	1+	76
F	2-	133
Mg	2+	72
Fe	0	126
Fe	2+	78
Fe	3+	64

TABLE II: Summary of relevant atomic and ionic radii from Shannon¹³ and Slater.¹⁴

* Fellow, Nanotechnology for Clean Energy IGERT

† Electronic address: bart@physics.rutgers.edu

‡ Current address: Institut Laue-Langevin, 71 avenue des Martyrs, 38000 Grenoble, France

¹ P. C. Graat and M. A. Somers, Applied Surface Science **100**, 36 (1996).

² M. Kasrai and D. Urch, J. Chem. Soc., Faraday Trans. 2 **75**, 1522 (1979).

³ A. Grosvenor, B. Kobe, M. Biesinger, and N. McIntyre, Surf. Interface Anal. **36**, 1564 (2004).

⁴ S. Rangan, R. Thorpe, R. A. Bartynski, M. Sina, F. Cosandey, O. Celik, and D. D. T. Mastrigiovanni, The

Journal of Physical Chemistry C **116**, 10498 (2012).

⁵ J. Ko, K. Wiaderek, N. Pereira, T. Kinnibrugh, J. Kim, P. Chupas, K. Chapman, and G. Amatucci, Appl. Mat. Interfaces **6**, 10858 (2014).

⁶ M. Sina, R. Thorpe, S. Rangan, R. Bartynski, G. Amatucci, and F. Consandey, In preparation (2014).

⁷ J. F. Watts and J. Wolstenholme, *An Introduction to Surface Analysis by XPS and AES* (2003).

⁸ C. Powell and A. Jablonski, *NIST Electron Effective-Attenuation-Length Database, Version 1.3, SRD 82* (National Institute of Standards and Technology, Gaithersburg, MD, 2011).

- ⁹ A. Jablonski and C. Powell, Surf. Sci. Rep. **47** (2002).
- ¹⁰ A. Jablonski and C. Powell, Surf. Sci. **520** (2002).
- ¹¹ C. Powell and A. Jablonski, Nucl. Instr. Meth. Phys. Res. **A601** (2009).
- ¹² J. Stout and S. Reed, J. Am. Chem. Soc. **76**, 5279 (1954).
- ¹³ R. Shannon, Acta Cryst. **A32**, 751 (1976).
- ¹⁴ J. Slater, J. Chem. Phys. **41** (1964).